

Preparation of TiO₂/Lignin Composites with *Agave sisalana* Residue for Bisphenol-A Removal

Aleir J. O. Silva,^a Franklin D. Xavier,^a Maria G. da Fonseca^b and Marta M. da Conceição^b *^c

^aPPGQ/CCEN, Universidade Federal da Paraíba, 58051-970 João Pessoa-PB, Brazil

^bDepartamento de Química, CCEN, Universidade Federal da Paraíba, 58051-970 João Pessoa-PB, Brazil

^cDepartamento de Tecnologia de Alimentos, Centro de Tecnologia e Desenvolvimento Regional, Universidade Federal da Paraíba, Av. dos Escoteiros, s/n, Mangabeira VII, 58058-600 João Pessoa-PB, Brazil

Composites prepared from metal oxides and materials derived from agroforestry residues have been successfully applied to remove emerging contaminants. The lignin properties, high surface area and number of functional groups, are beneficial in the preparation of TiO₂ composites. In the present work, sisal residue was used as a source of lignin, and after extraction, the lignin was applied in the preparation of an adsorbent composite with TiO₂ to remove bisphenol-A. The optimal conditions for lignin extraction resulted in a lignin purity of 73%. Characterization proved that the synthesized composites have a high surface area (> 100 m² g⁻¹), homogeneous distribution of TiO₂ particles and stable surface charge. Such characteristics resulted in a lignin/TiO₂ composite with a maximum adsorption capacity of 13.7 mg L⁻¹, capable of removing up to 97% of bisphenol-A. The adsorbent can be used in six cycles, removing over 70% by the third cycle, which indicates good stability.

Keywords: renewable carbon, reuse, emerging contaminant

Introduction

The *Agave sisalana* plant, popularly known as sisal, is an herbaceous plant belonging to the Agavaceae family. In Brazil, this species is widespread in the Caatinga biome and is cultivated mainly to obtain fibers for the production of ropes and handicrafts; however, only 5% of the weight of the plant is used for this purpose, and the byproduct, which includes solid residue, is discarded and becomes an environmental problem.¹ The solid residue is a material rich in cellulose, hemicellulose and lignin.² Each of these three components can be extracted and applied in different areas. Lignin can be extracted from this residue by sequential chemical processes and applied, for example, in the preparation of adsorbent materials for emerging contaminants.^{3,4}

Lignin is an aromatic copolymer found in plant walls that contains several functional groups in its structure, including aliphatic hydroxyls, phenolic hydroxyls, methoxyls and carbonyls. These groups contribute to its chemical reactivity and application in high-value products.⁵

Lignin in its raw form can be used as an adsorbent to remove pollution in wastewater, as it has oxygen functional groups that can adsorb heavy metal ions through ion exchange and chelation.⁶ However, due to its intertwined and three-dimensional structure, raw lignin has little efficiency for removing heavy metals and other organic contaminants. In general, to make it more effective in the adsorption process, the lignin is thermally and/or chemically modified to improve its biosorption capacity.⁷

One of the strategies for modifying lignin is to combine it with materials that have different physical and chemical properties.⁷ The presence of reactive functional groups in lignin allows it to be modified by chemical reactions such as sulfonation, oxidation, amination, condensation and copolymerization. Such modification can increase the spatial network, the content of hydroxyl and carboxyl groups or introduce other functional groups that provide the prerequisite for lignin to become a low-cost and high-performance adsorbent material.⁷ The combination of the properties of lignin with those of TiO₂ is capable of producing a material with high adsorption capacity for the bisphenol-A (BPA) molecule. The addition of TiO₂ nanoparticles to lignin will promote a greater surface area, as the nanoparticles will disperse along the surface, forming

*e-mail: martamaria8@yahoo.com

Editor handled this article: Célia M. Ronconi (Associate)



smaller lignin-TiO₂ clusters and increasing the surface area and number of active sites.³ Furthermore, the negative surface of TiO₂ nanoparticles can promote electrostatic attractions within the structure of the BPA molecule over a wide pH range.

TiO₂ is already widely applied in the field of photocatalytic degradation, as it is considered a good semiconductor, does not present toxicity and has low cost and good stability.⁸ However, its use is limited in photocatalysis due to its poor performance under visible light. Therefore, the combination of TiO₂ and lignin has been applied to improve photocatalytic performance in visible light conditions.⁹ In order for the composite material to function properly in photodegradation, it is necessary to subject the lignin to a quaternization process, the objective of which is to add positive charges to the structure so that it binds to the negative structure of TiO₂.¹⁰ However, the quaternization process requires the use of membranes for purification, which makes the process expensive and complex.

On comparing photocatalysis and adsorption processes for removing BPA, adsorption is more promising because the use of TiO₂ as a photocatalyst is limited in that it only has good efficacy in UV light. Although other materials, including lignin, can enhance its capacity as a photocatalyst in visible light, the extent of photocatalysis in the degradation of emerging contaminants is still inferior to the removal of contaminants by adsorption.

Lignin has also been incorporated into metal oxides, as in the preparation of a magnetic adsorbent with aminated lignin/CeO₂/Fe₃O₄ (Al-NH₂@Fe₃O₄-Ce), having high affinity for phosphate and easily separated from aqueous solutions.¹¹ Another application is the preparation of a lignin/TiO₂ composite with antimicrobial properties.¹² An effective alternative is lignin/TiO₂ composite applied for removing organic pollutants through adsorption. TiO₂ has already been incorporated into a chitosan-lignin mixture, generating a material with good performance in the adsorption of glossy black dye molecules.⁴ A lignin/TiO₂ composite has also been prepared and used for Pb^{II} sorption.¹³

Among the emerging contaminants is 2,2-bis(4-hydroxyphenyl)propane, commonly called bisphenol-A (BPA). BPA is a synthetic organic compound belonging to a group of diphenylmethane derivatives and bisphenols that is used as an additive in the production of polycarbonate plastics and epoxy resins. BPA is classified as an endocrine-disrupting compound because of its estrogenic characteristics.¹⁴ In freshwater bodies around the world, BPA is generally found at levels of around 1.0 µg L⁻¹.¹⁵ However, it is found in higher concentrations in Brazil (3.01 µg L⁻¹) and China (44.65 µg L⁻¹).^{16,17}

There are currently many methods for removing BPA from wastewater, such as nanofiltration,¹⁸ reverse osmosis,¹⁹ advanced oxidation processes,²⁰ ozonation²¹ and the use of membrane bioreactors.²¹ However, adsorption is considered an alternative to these methods, providing effective and rapid removal of pollutants along with low operational costs, a simple easy-to-use design and less production of harmful by-products.²² Among the materials used to remove BPA through adsorption are clays and clay materials, nanomaterials, graphene, activated carbon, printed polymers and agricultural waste.²³ To our knowledge, there are no reports on the use of a lignin/TiO₂ composite to remove BPA exclusively through adsorption.

At the time of writing, no studies have yet been reported using lignin extracted from sisal in the preparation of a lignin/TiO₂ adsorbent composite for the removal of BPA. Therefore, the objective of this work was to extract lignin from sisal solid waste and reuse it to give it high added value and reduce the environmental impact generated by its disposal, in addition to providing a renewable and sustainable carbon source. Although *Agave sisalana* is widely cultivated in the northeast region of Brazil and its cultivation is the main source of income for several municipalities in this region, only its fibers have high added value, with the residue having to be discarded. Thus, the use of this residue for lignin extraction adds value, in addition to reducing the environmental impact caused by its disposal.

Furthermore, incorporating TiO₂ into the lignin-derived carbonaceous matrix takes advantage of the characteristics of the lignin (good porosity, oxygen functional groups on its surface and good thermal stability) and TiO₂ (thermal stability, low cost and non-toxic), enabling its application as a composite capable of effectively removing BPA.

Experimental

Materials and reagents

The solid sisal residue was purchased in the municipality of Nova Floresta in the state of Paraíba, Brazil. The reagents used with a high degree of purity were sulfuric acid (99%), sodium hydroxide (99%), ethanol (99%), cyclohexane (99%) and acetic acid (99.7%), all obtained from Vetec, São Paulo, Brazil. Sodium chlorite (99%), titanium butoxide (99%), and BPA were purchased from Sigma-Aldrich (Barueri, Brazil). Adsorption tests were carried out using deionized water.

Lignocellulosic characterization

The sisal residue was dried at 50 °C in a Tecnal TE390

stove (Piracicaba, Brazil). The samples were ground in a Solab SL-31 mill and sieved using a 60-mesh Tyler sieve (Mentor, USA). Following TAPPI (Technical Association of the Pulp and Paper Industry) standards, the percentages of the lignocellulosic constituents were determined: holocellulose, alpha-cellulose, Klason lignin and ash, adapted from TAPPI T19 M-54, TAPPI 203 cm-99, TAPPI 222 and TAPPI 413 om-11, respectively.²⁴

Lignin extraction

An acid pretreatment on sisal waste was carried out according to concentration, temperature and reaction time conditions that had been determined in a previous study.²⁵ All acid pretreatment and lignin extraction tests were carried out in a Biofoco stainless-steel reactor (São Paulo, Brazil). Following acid treatment, the lignin was extracted with a sodium hydroxide solution and precipitated by adjusting the pH of the solution to 2.0.

To evaluate the best conditions for lignin extraction, a 2³ design plan was carried out with three central points (to evaluate the effects of sodium hydroxide concentration, hydrolysis time and temperature), whose response was the percentage purity of lignin obtained by the Klason method adapted from TAPPI 222 standard. The experimental planning matrix with coded and real levels of planning conditions is shown in Tables 1 and 2.

Table 1. Experimental planning matrix with coded levels for lignin extraction

Experiment	NaOH concentration / %	Hydrolysis time / min	Temperature / °C
1	-1	-1	-1
2	+1	-1	-1
3	-1	+1	-1
4	+1	+1	-1
5	-1	-1	+1
6	+1	-1	+1
7	-1	+1	+1
8	+1	+1	+1
9	-1.68	0	0
10	1.68	0	0
11	0	-1.68	0
12	0	1.68	0
13	0	0	-1.68
14	0	0	1.68
15	0	0	0
16	0	0	0
17	0	0	0

Table 2. Real and coded levels of the input variables of the experimental design for lignin extraction

Variable	-1	0	+1
NaOH concentration / %	1.5	2.0	2.5
Hydrolysis time / min	10.0	30.0	50.0
Temperature / °C	80.0	100.0	120.0

Preparation of composites

Titanium(IV) butoxide (8 mL) and ethanol (21 mL) were added to a beaker and mixed for 1 h; the solution was then added to a mixture of deionized water (40 mL) and lignin (1:8, 0.5:8 and 0.25:8 mass volume for lignin/TiO₂) and stirred vigorously for 4 h at 80 °C. The solid was vacuum filtered, washed abundantly with deionized water and dried in an oven at 60 °C for 12 h. Finally, the solid was disaggregated and calcined at 500 °C for 2 h in a nitrogen atmosphere. As a control sample, TiO₂ was synthesized using the same steps but without the addition of lignin.^{26,27}

Characterization of composites

All materials were subjected to Fourier transform infrared spectroscopy (FTIR) on a Shimadzu spectrophotometer (Tokyo, Japan) using the KBr pellet method in the region 4000-400 cm⁻¹. To identify the crystalline phases and crystallite size, X-ray diffraction (XRD) was carried out in the 2θ range of 20-90° with Cu Kα radiation (λ = 1.5406 Å) in a Shimadzu (Model ZRD-6000, Tokyo, Japan) diffractometer with a power of 2 kVA, voltage of 30 kV and current of 30 mA at a rate of 2° min⁻¹. Crystallite size was calculated using the Scherrer formula (equation 1):²⁸

$$D = \frac{K\lambda}{\beta \cos\theta} \quad (1)$$

where K is the Scherrer constant, λ is the wavelength of the X-rays, β is the full width at half-maximum of the peak and θ is the Bragg angle.

The porosity of the materials was analyzed with nitrogen adsorption-desorption isotherms collected at 77 K using the Micromeritics Accelerated Surface Area and Porosimetry System (Model ASAP 2420, Norcross, United States). Prior to analysis, the samples were subjected to heat treatment at 100 °C for 2 h. The zeta potential was measured using Malvern Zetasizer Nano equipment (Malvern, United Kingdom). The average particle size was obtained by transmission electron microscopy (TEM) using FEI (Model Tecnai G2, Stanford, United States)

equipment operating at an acceleration voltage of 100 kV. The morphology was analyzed by scanning electron microscopy (SEM). The samples were metallized with gold and analysis was carried out using a Quanta FEI 450 (Model EDS Bruker, Prague, Czech Republic) instrument at a voltage of 10 kV.

Adsorption tests

A stock solution of 100 mg L⁻¹ BPA was prepared and subsequently diluted to concentrations between 10 and 50 mg L⁻¹, according to in a previous study carried out for BPA adsorption.²⁸ The adsorption tests were carried out at 30 °C with stirring at 200 rpm in a Tecnal TE-4200 shaker (Piracicaba, Brazil). Tests to verify the influence of pH on the adsorption process were carried out with a solution of 10 mg L⁻¹ BPA in pH range 2-12. The pH of the solution was adjusted with solutions of 0.1 mol L⁻¹ HCl and 0.2 mol L⁻¹ NaOH.

The effect of the initial dosage of adsorbent was developed with a solution of 10 mg L⁻¹ BPA in dosages of 0.5, 1.0, 1.5 and 2.0 g L⁻¹ at pH 6. To investigate the influence of contact time on adsorption, the BPA solutions were adjusted to pH 6 and shaken, with aliquots removed at contact times of 30, 60, 120 and 180 min. To evaluate the effect of the initial concentration of pollutant, solutions were used at concentrations of 10, 20, 30, 40 and 50 mg L⁻¹ BPA, with the pH adjusted to 6. In all tests, the solution was separated from the solid using centrifugation. BPA was quantified in aqueous solution by absorption spectrometry in the visible ultraviolet region on a UV-Vis spectrometer (Shimadzu Model UV-2550, Tokyo, Japan) at 224 nm.²⁹

The amount of adsorbed BPA (*q*) and the pollutant removal efficiency (*R*) by the adsorbent were determined using equations 2 and 3, respectively:

$$q = \frac{(C_i - C_e)V}{m} \quad (2)$$

$$R(\%) = \frac{(C_i - C_e)}{C_i} \times 100 \quad (3)$$

where *C_i* and *C_e* are the initial and equilibrium BPA concentration (mg L⁻¹), respectively, *m* is the mass of adsorbent (g) and *V* (mL) is the volume of the solution. The equilibrium isotherms were analyzed with the Freundlich³⁰ and Langmuir³¹ as defined in equations 4 and 5, respectively:

$$\text{Freundlich} \quad q_e = K_F C_e^{\frac{1}{n}} \quad (4)$$

$$\text{Langmuir} \quad q_e = \frac{q_{\max} K_L C_e}{1 + K_L C_e} \quad (5)$$

where *C_e* (mg L⁻¹) is the BPA equilibrium concentration and *q_e* (mg g⁻¹) is the equilibrium BPA amount adsorbed on the solid. In the Freundlich equation, *K_F* (mg g⁻¹) (mg L⁻¹)^{-1/n} and *n* are Freundlich constants related to the capacity and intensity of adsorption, respectively. In the Langmuir equation, *q_{max}* (mg g⁻¹) is the maximum adsorption capacity of the adsorbent, assuming monolayer drug uptake by the adsorbent, and *K_L* (L mg⁻¹) is the Langmuir constant.

Kinetic data were analyzed by using pseudo-first-order³² and pseudo-second-order³² models (equations 6 and 7, respectively):

$$q_t = q_e (1 - e^{-k_1 t}) \quad (6)$$

$$q_t = \frac{q_e^2 k_2 t}{1 + k_2 t} \quad (7)$$

where *q_e* and *q_t* are the adsorption capacities (mg g⁻¹) at equilibrium and at time *t* (min), respectively, and *k₁* (min⁻¹) and *k₂* (g mg⁻¹ min⁻¹) are the pseudo-first-order and pseudo-second-order rate constants, respectively.

Preliminary tests were carried out with the carbonaceous material derived from lignin under the following conditions: pH = 6, time = 180 min, BPA concentration = 10 mg L⁻¹ and adsorbent concentration = 2 g L⁻¹. However, no adsorption of BPA was observed, whereas under the same conditions an adsorption capacity was observed with the composites and pure TiO₂.

Reuse of composites

The reuse of solid was evaluated for six adsorption cycles using methanol as the desorbing agent, according to a previous procedure.³³ Samples (100 mg) of 0.5 g-lignin/TiO₂ loaded with BPA were washed with 20 mL of methanol, under agitation, for 2 h at 30 °C. Before reuse, the recycled adsorbents were washed with distilled water and dried at 50 °C. For each adsorption cycle, the initial BPA concentration was 10 mg L⁻¹ and adsorption was performed as described in the previous section.

Results and Discussion

Lignocellulosic composition

The percentages obtained from the main constituents of the lignocellulosic biomass of sisal residue are presented in Table 3. The values determined from the lignocellulosic composition analyses in accordance with the TAPPI standards for lignocellulosic procedures indicate significant amounts of lignin, at around 15.5%. These values are

similar to those obtained for some of the most currently abundant sources of lignocellulosic biomass, such as sugar cane bagasse (18%), corn straw (11-19.1%), rice straw (17-19%) and wheat straw (12-16%),^{34,35} which shows that sisal residue is an excellent source of lignin.

Table 3. Lignocellulosic composition of sisal residue

Composition	Content / %
Moisture	8.4
Ash	14.0
Extractives	6.0
Lignin	15.5
Cellulose	37.2
Hemicellulose	16.7

Lignin extraction

To evaluate the effectiveness of lignin extraction from sisal residue using the alkaline method, a 2³ experimental design was analyzed with three central points where the measured response was the purity of the lignin obtained at the end of each proposed extraction condition, using the method by Klason. With this alkaline treatment, hemicellulose fractions can be recovered alongside the lignin components.

Using the experimental data obtained in Table 4, statistical analysis was carried out to investigate the influence of concentration, temperature and time on the lignin purity response.

The Pareto chart (Figure 1) is widely used to represent the significance of parameters and their interactions in experimental designs. The horizontal bars display the importance of the factors (input variables) to the proposed experimental design in descending order. Any parameter that crosses the dashed line is considered significant according to the confidence level adopted, which in this case is 95% or $\alpha = 0.05$.^{25,36}

For the lignin percentage, all input variables were statistically significant, with a confidence level of 95%. Because the effect values were positive, the higher the concentration, time and temperature values, the greater the purity of the lignin obtained in the experimental range studied. Another important point to highlight is the interaction between temperature and time, which was statistically significant, meaning that the interaction between them causes a directly proportional effect to obtain lignin with a higher degree of purity.³⁷

The analysis of variance (ANOVA) for the lignin purity response was realized by considering the parameters that were significant. According to the F test value, where

Table 4. A 2³ experimental design with three central points where the measured response was the purity of the lignin

Experiment	NaOH concentration / %	Hydrolysis time / min	Temperature / °C	Purity / %
1	-1	-1	-1	42.0
2	+1	-1	-1	53.9
3	-1	+1	-1	39.5
4	+1	+1	-1	54.1
5	-1	-1	+1	61.2
6	+1	-1	+1	62.0
7	-1	+1	+1	58.8
8	+1	+1	+1	73.0
9	-1.68	0	0	47.3
10	1.68	0	0	56.2
11	0	-1.68	0	46.0
12	0	1.68	0	58.8
13	0	0	-1.68	51.6
14	0	0	1.68	62.2
15	0	0	0	63.1
16	0	0	0	69.5
17	0	0	0	64.6

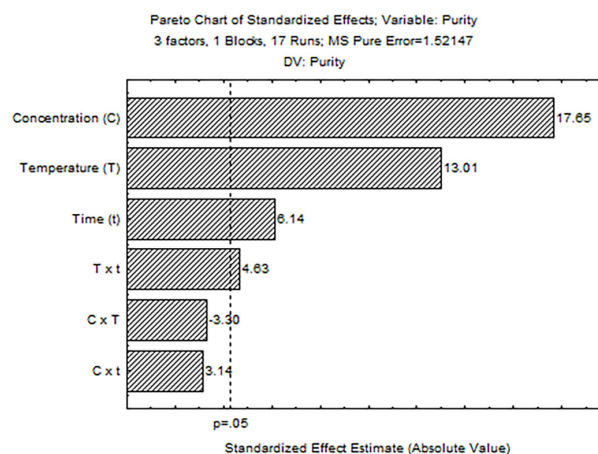


Figure 1. Pareto chart used to assess the significance of the parameters and their interactions.

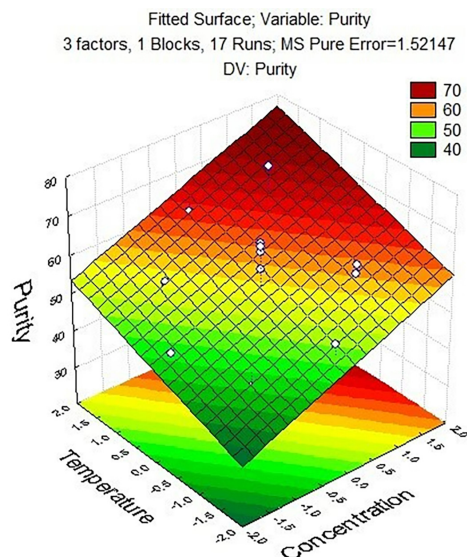
$F_{cal} > F_{tab}$, the model was statistically significant for a confidence level of 95% and a coefficient of determination of 85.74% (Table 5).

Because the model was significant, it was possible to obtain the regression model for the proposed experimental design, as well as highlighting the effectiveness of alkaline treatment for removing lignin.³⁷ On evaluating the response surface generated in relation to the effects of the input variables, the maximum purity of the lignin is obtained when both the concentration and temperature are at maximum (Figure 2).

Table 5. Linear regression model and *F* test value for the lignin purity

Regression model	R ²	<i>F</i> test (F_{cal}/F_{tab})
Purity = 56.46 + 5.89C + 2.05t + 4.34T + 2.02tT	85.74	1.61 (5.26/3.26)

C: NaOH concentration; T: temperature; t: time; R²: coefficient of determination.

**Figure 2.** Response surface in relation to lignin purity.

Experimental test 8 encompassed the ideal conditions for extracting lignin from sisal residue with the highest purity (73%). Values for concentration (2.5% sodium hydroxide), temperature (120 °C) and time (50 min) were at a maximum in the experimental range analyzed.

Characterization of composites

Structural and morphological properties

The results of XRD analysis are presented in Figure 3a. The indexing of reflection plans was carried out in accordance with PDF file 00-021-1272. For all systems investigated, the formation of anatase was observed, regardless of the amount of lignin used. Diffraction data were indexed in reflection planes 101, 004, 200, 105, 211, 204, 116, 220, 215 and 224.²⁶

The average crystallite sizes (*D*) calculated by Scherrer's equation are provided in Table 6. When comparing the crystallite size, it is possible to verify that there was a decrease with the addition of lignin, as it is predicted that a smaller crystallite size in C/TiO₂ composites indicates the presence of carbon in the crystalline structure of TiO₂.²⁷ Therefore, the insertion of lignin as a carbon source was more effective in the 0.5 g-lignin/TiO₂ composite, which contains an intermediate amount of lignin.

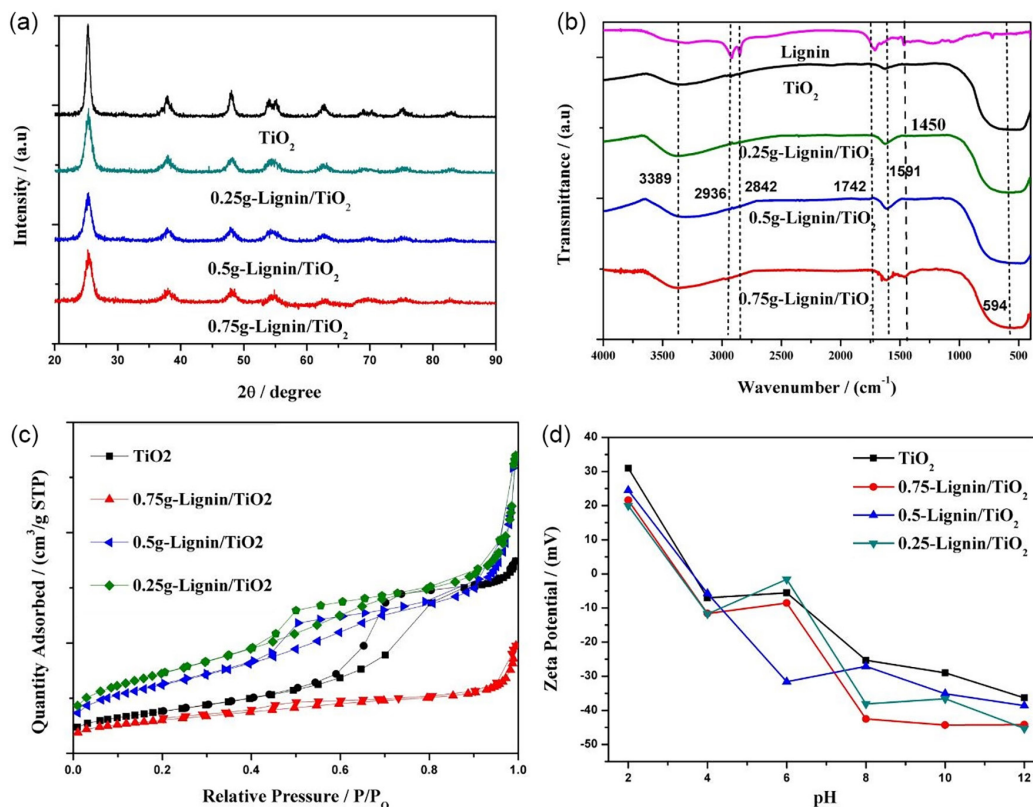
**Figure 3.** (a) X-ray diffraction patterns, (b) Fourier transform infrared (KBr) spectra, (c) nitrogen adsorption-desorption isotherms and (d) zeta potential measurements for the precursors and their composites.

Table 6. Calculated values of surface area and crystallite size (D)

Material	Surface area / (m ² g ⁻¹)	D / nm
TiO ₂	82.0	9.4
0.75 g-Lignin/TiO ₂	64.0	4.2
0.5 g-Lignin/TiO ₂	134.0	4.0
0.25 g-Lignin/TiO ₂	157.0	5.9

Figure 3b shows the FTIR spectra for lignin extracted from sisal, TiO₂ and the synthesized composites. It is possible to observe characteristic bands of lignin in the spectrum, such as the one at 1450 cm⁻¹, which is attributed to aromatic rings and phenolic functional groups of the guaiacyl units. The band at 1742 cm⁻¹ is associated with C=O stretching and the peaks at 2842 and 2936 cm⁻¹ are due to C–H stretching of side chains linked to aromatic rings (–OCH₃, –CH₃ and –CH₂–).^{5,38} On observing the spectra of the synthesized materials, it is possible to verify a band at 594 cm⁻¹, which is related to the Ti–O and Ti–O–Ti bonds and can be attributed to the formation of the anatase phase in TiO₂ and in the composites.³⁹ The band at 1591 cm⁻¹ indicates Ti–OH bonds and CO stretching;⁴⁰ this band increases in intensity in the lignin/TiO₂ composite, which indicates interaction between the functional groups of lignin and TiO₂.⁴¹ The band at 3389 cm⁻¹ is attributed to water molecules adsorbed on surfaces but is also related to –OH stretching of hydroxyl groups on the surface of the composites.⁴²

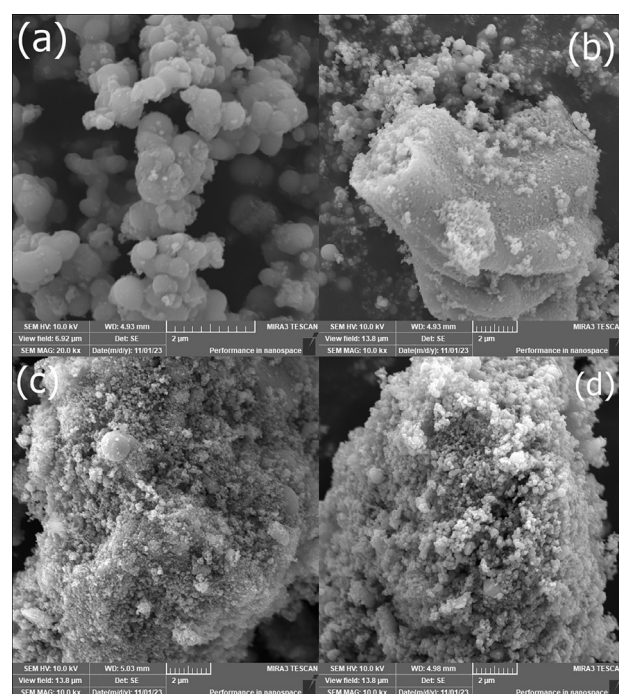
The results for the nitrogen adsorption-desorption isotherms and surface area are shown in Figure 3c and Table 6. The adsorption-desorption isotherms of the four synthesized materials are Type IV, which classifies them as belonging to a group of materials with a mesoporous structure, which is the type of porosity most suitable for adsorbing organic contaminant molecules.⁴⁰ The two composites with smaller amounts of lignin (0.5 g-lignin/TiO₂ and 0.25 g-lignin/TiO₂) presented the largest surface areas; as expected, the addition of lignin to TiO₂ increased the surface area, enabling an increase of active sites to adsorb BPA. However, at 0.75 g-lignin/TiO₂ there was a decrease in surface area, which may have been caused by pore blockage due to excess carbon.⁴³

The zeta potential measures the surface charge of a compound and the values measured for the precursors and their composites are shown in Figure 3d. The nanoparticles will tend to agglomerate when the zeta potential is close to 0 mV due to the absence of a strong mutual repulsion. On the other hand, when the absolute value of the zeta potential is greater than 30 mV (greater than +30 mV or less than –30 mV), the nanoparticles present uniform dispersion in the solution due to the strong mutual repulsion of the surfaces.⁴⁴ The materials presented values greater

than +30 mV and less than –30 mV but only at a few pH values, indicating that uniform dispersion of the charges will depend on the pH. Furthermore, it should be noted that all the materials presented a negatively charged surface at almost all of the pH values.

As shown in Figure 3d, different behaviors occur in the materials as the composition varies. At pH 6, the 0.5 g-lignin/TiO₂ composite showed the lowest zeta potential (–31.6 mV), indicating that among the materials at this pH the negative charges are distributed more evenly. Furthermore, it appears that at pH 2 all solids have a positive potential, which indicates that the surfaces are protonated due to the low pH value. As the pH increased, surface deprotonation occurred and the negative charges of TiO₂ and other negative groups dominated, leading to a negative zeta potential.

Figure 4a shows that the TiO₂ particles formed by the titanium butoxide precursor, as predicted, have a spherical shape that may be related to the high BET surface area for this material. From Figure 4b, it is possible to verify the morphology of the composites and how the percentage lignin addition affected the surfaces. Figure 4b shows very heterogeneous particle shapes and sizes, including regions with isolated titanium particles and few titanium particles on the lignin surface. For samples obtained with smaller amounts of lignin (Figures 4c and 4d), a more uniform distribution of the titanium particles is observed. Furthermore, it is possible to observe that with the addition

**Figure 4.** Scanning electron micrographs of (a) TiO₂, (b) 0.75 g-lignin/TiO₂, (c) 0.5 g-lignin/TiO₂ and (d) 0.25 g-lignin/TiO₂.

of lignin, many of the titanium particles decreased in size. From the image obtained by TEM (Figure 5), it was possible to calculate the average particle size for the 0.5 g-lignin/TiO₂ composite, which was around 10 nm, confirming that this composite has particle sizes on the nanometer scale. This value is similar to that found in another study that used TiO₂ in a carbonaceous matrix, which produced a material with an average particle size of 11 nm.⁴⁵

Adsorption tests

Effect of initial adsorbent dosage

The effect of the initial adsorbent dosage for the four synthesized materials can be seen in Figure 6a. For practical purposes, the effects of contact time, initial BPA concentration and pH on TiO₂ were not investigated because the BPA removal for this material was not significant. The gradual increase in BPA removal followed the increase in adsorbent concentration in the medium; this effect is observed in the 0.5 g-lignin/TiO₂ composite, whose removal was around 90% at an adsorbent concentration of 2 g L⁻¹. The increasing removal efficiency of this composite is caused by the increase in surface area and number of adsorption sites as the adsorbent dosage increases. However, BPA removal is lower for the other three materials. This can be justified by the distribution of particles and charge on the surface of the materials. As seen in the SEM analyses (Figure 4), the 0.5 g-lignin/TiO₂ composite showed a more uniform distribution of TiO₂ particles on the lignin surface, which favored an increase in the number of active sites in the material, thus capturing more molecules of BPA.

Effect of pH

In the chemical speciation diagram for BPA (Figure 7a), up to pH 7 the molecule remains in its non-ionized form, whereas the anionic forms, BPA⁻ and BPA²⁻ (Figure 7b), are predominant in the pH range 7-12. Therefore, it is

possible to explain the adsorption behavior of materials by looking at the zeta potential measurements. Up to pH 7, the neutral BPA species interacts with the negatively charged surface of the materials through hydrogen bond interactions and interactions between lignin residues, which will be discussed in the FTIR analysis of the solids after adsorption. As the pH increases, anionic BPA species emerge, causing repulsive electrostatic interactions between the negative surface of the material and the BPA molecule.

Among the three composites, 0.5 g-lignin/TiO₂ showed greater removal in the pH range 2-8 (Figure 6b), especially in the neutral pH range (6-7) with a pK_a of around 9.6, where BPA has high hydrophobicity and lipid permeability, which generates bioaccumulation in living organisms.⁴⁷ The maximum removal of BPA by this composite occurs at pH 6-7, whereas the maximum removal of other composites occurs at pH 8 but at a lower percentage. Therefore, the 0.5 g-lignin/TiO₂ composite was the most suitable material for removing BPA in a pH range close to neutrality because the negative charges are distributed more uniformly over the surface, as verified by the zeta potential measurements (Figure 3d). However, from pH 10 onwards, a drastic decrease in removal is noted, as BPA is mostly in its anionic form at this pH (Figure 7b) and, consequently, the negative surface of the composites will repel the BPA molecule, preventing significant removal.

Effect of removal time

Figure 6c elucidates the variation in BPA removal with removal time. As expected, in 0.5 g-lignin/TiO₂, removal occurred with increasing contact time up to 180 min, with around 97% removal, which makes this time sufficient to remove almost all of the BPA from the medium. In the other two composites, removal occurs more slowly and stabilizes after 180 min, which indicates that the number of active sites decreased over a shorter period and reached saturation more quickly.

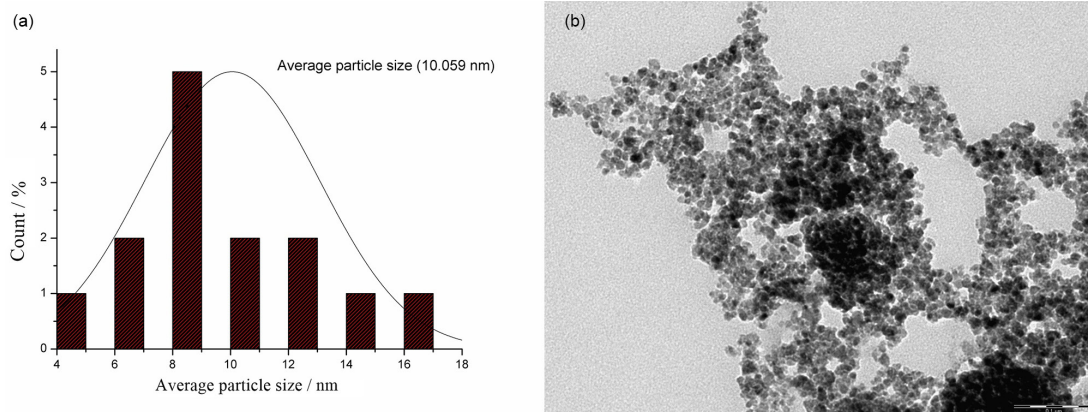


Figure 5. Average particle size distribution for the 0.5 g-lignin/TiO₂ composite.

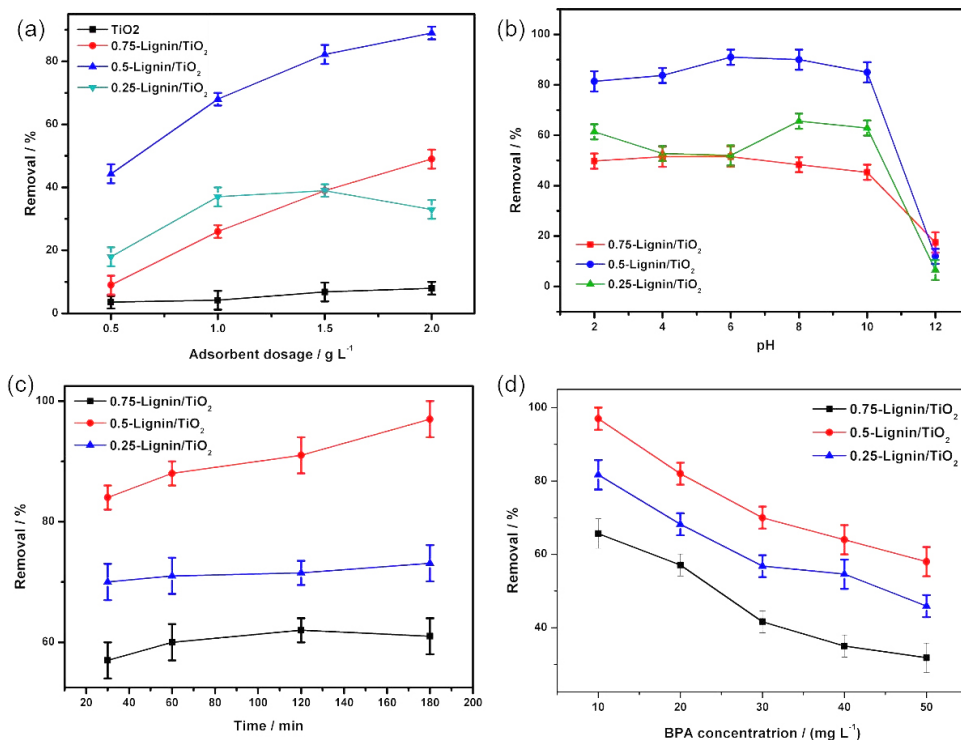


Figure 6. (a) Effect of adsorbent dosage at concentrations of 0.5, 1.0, 1.5 and 2 g L⁻¹; (b) effect of pH on bisphenol-A (BPA) removal in the pH range 2-7; (c) effect of removal time, at times of 30, 60, 120, and 180 min; and (d) effect of the initial concentration of BPA, at concentrations of 10-50 mg L⁻¹.

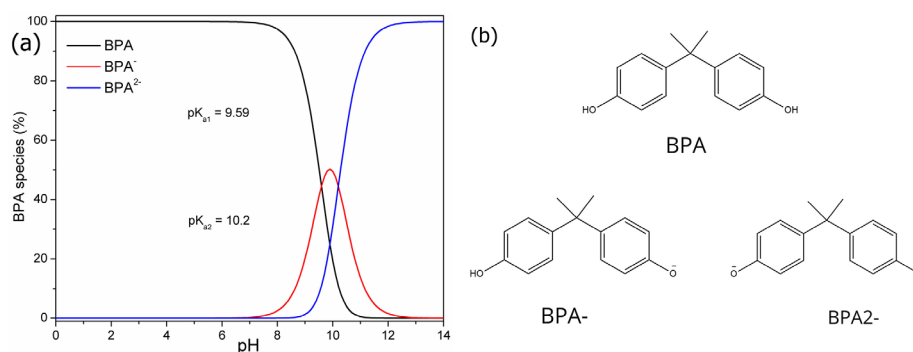


Figure 7. Chemical speciation diagram for: (a) bisphenol-A (BPA)⁴⁶ and (b) BPA and its anionic forms.

Effect of initial BPA concentration

The composites showed a decrease in removal efficiency with increasing BPA concentration in the medium (Figure 6d). At 0.5 g-lignin/TiO₂, the calculated maximum adsorption capacity was 13.7 mg g⁻¹. This value is higher than that obtained by other materials, such as 3.54 mg g⁻¹ for commercial granulated activated carbon, whose adsorption process consisted of using solutions of 10-400 mg L⁻¹ BPA and 20 g L⁻¹ adsorbent for 120 min of adsorption.⁴⁸ Rice husk ash was also used in the adsorption of BPA, where a maximum adsorption capacity of 8.72 mg g⁻¹ was obtained using solutions of 10-400 mg L⁻¹ BPA and 30 g L⁻¹ adsorbent for an adsorption time of 180 min.⁴⁸

Adsorption isotherms

Langmuir (Figure 8a) and Freundlich (Figure 8b) adsorption models were used to describe the interaction between BPA and the 0.5 g-lignin/TiO₂ composite, which showed the better adsorption performance.

The Langmuir isotherm model states that adsorption occurs in a monolayer, assuming that each adsorbate molecule occupies a site and the adsorption energy is uniform on the surface, whereas the Freundlich model assumes that the adsorbent surface is heterogeneous and adsorption occurs in multilayers.⁴ The correlation coefficient (R²) of the Freundlich model was 0.98, whereas for the Langmuir model it was 0.72; therefore, the isotherm model with the better fit is the Freundlich model, indicating that the process

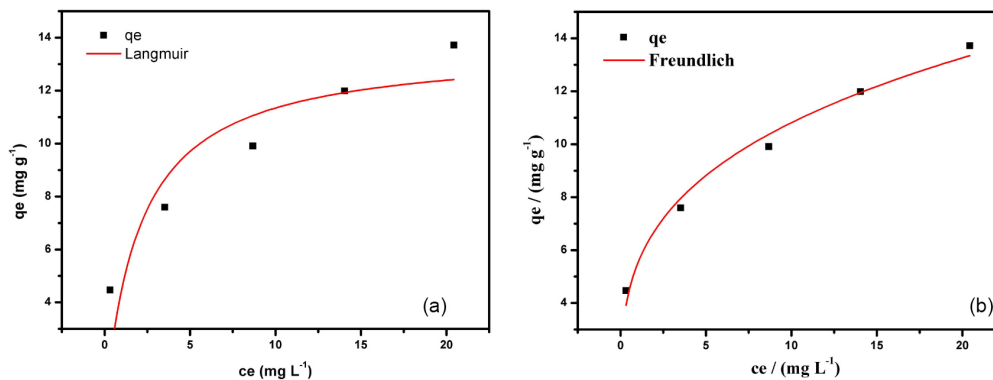


Figure 8. Langmuir (a) and Freundlich (b) isotherm models applied to the adsorption of bisphenol-A on 0.5 g-lignin/TiO₂.

is dominated by multilayer adsorption.³⁶ The values of the parameters calculated by the isotherm models are described in Table 7. K_F is the adsorption constant of the Freundlich model associated with the adsorption capacity of BPA by the composite. The K_F value is < 1 , thus indicating favorable sorption. The n value represents the heterogeneity surface. The combined results indicated the adsorption capacity of the heterogeneous surface.

Table 7. Values of the parameters calculated by the isotherm models

Isoterm models	Parameter	Value
Langmuir	$q_{\max, \text{exp}} / (\text{mg g}^{-1})$	13.70
	$q_{\max, \text{cal}} / (\text{mg g}^{-1})$	13.66
	$K_L / (\text{L mg}^{-1})$	0.49
	R^2	0.72
Freundlich	$K_F / ((\text{mg g}^{-1}) (\text{L mg}^{-1})^{1/n})$	0.29
	n	3.40
	R^2	0.98

q_{\max} : maximum adsorption capacity of the adsorbent; K_L : Langmuir constant; K_F and n are Freundlich constants related to the capacity and intensity of adsorption, respectively; R^2 : coefficient of determination.

The results of the calculated parameters were compared with literature data, highlighting the adsorption potential of the 0.5 g-lignin/TiO₂ composite obtained in the present study (Table 8).

Adsorption mechanism

In Figure 9a, the two bands marked in the FTIR spectrum (1616 and 1447 cm^{-1}) correspond to the functional groups $-\text{COOH}$ and $-\text{OH}$, respectively.⁵⁰ The appearance of the band at 1447 cm^{-1} indicates that the material adsorbed BPA on the surface. The wavenumber shift from 3358 to 3396 cm^{-1} suggests the formation of hydrogen bonds between the $-\text{OH}$ or $-\text{COOH}$ functional groups of the composite and the BPA functional groups ($-\text{OH}$).⁴⁰

The XRD patterns of the material before and after

Table 8. Comparison of adsorption parameters for BPA in different materials

Material	$K_F / ((\text{mg g}^{-1}) (\text{L mg}^{-1})^{1/n})$	n	Reference
0.5 g-Lignin/TiO ₂	0.29	3.40	this study
Activated carbon	20.80	1.53	Supong <i>et al.</i> ⁴⁹
CoFe ₂ O ₄ @SiO ₂ -P4VP	0.86	0.92	Valentini <i>et al.</i> ⁴⁷
Rice husk ash	0.65	–	Sudhakar <i>et al.</i> ⁴⁸

K_F and n are Freundlich constants related to the capacity and intensity of adsorption, respectively.

adsorption are shown in Figure 9b. It is possible to observe that there was no change in the crystalline structure of the material after adsorption. Furthermore, it was not possible to verify the presence of the (002) and (100) planes at $2\theta = \text{ca. } 23$ and 43° , which correspond to a microcrystalline structure similar to graphite.⁴⁹ Therefore, there is no evidence of the occurrence of π - π type interactions that could occur between the π electrons of the benzene ring of BPA and the sp^2 graphitic carbon of the composite.

Adsorption kinetics

Pseudo-first-order and pseudo-second-order kinetic models were used to evaluate the adsorption kinetics of BPA on the 0.5 g-lignin/TiO₂ composite (Figure 10).

The results indicated that the adsorption kinetics of BPA were better adjusted to the pseudo-second-order kinetic model (Table 9). These results are in agreement with those from previous studies on BPA removal by various adsorbents, including studies by Hao *et al.*,⁵¹ Shi *et al.*⁵² and Yousefinia *et al.*⁵³

Reusability of adsorbent

An ideal adsorbent should have good adsorption capacity even after many reuse cycles. This process is

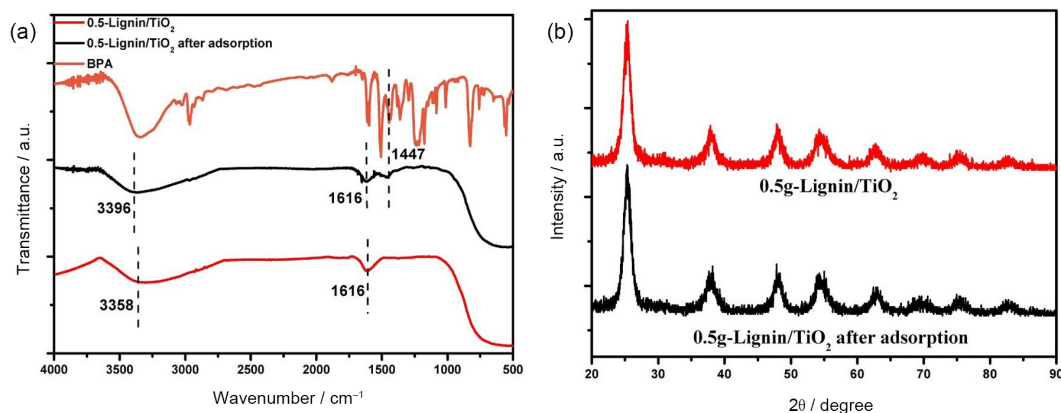


Figure 9. Fourier transform infrared (KBr) spectra (a) and X-ray diffractograms (b) of the 0.5 g-lignin/TiO₂ composite before and after bisphenol-A adsorption.

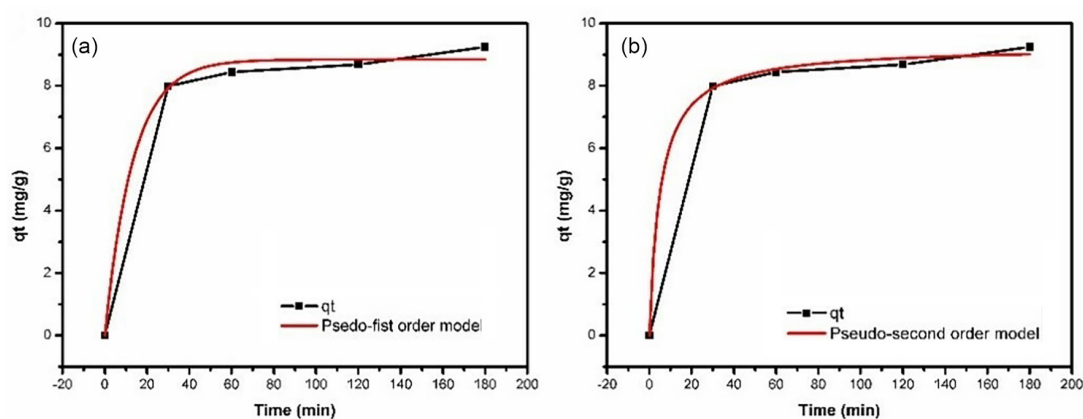


Figure 10. Kinetic models applied for the adsorption of bisphenol-A by 0.5 g-lignin/TiO₂ (a) pseudo-first-order and (b) pseudo-second-order.

Table 9. Parameters calculated for the kinetic models

Kinetic model	Parameter	Value
Pseudo first order	R ²	0.994
Pseudo second order	R ²	0.997

R²: coefficient of determination.

capable of reducing costs and avoiding the generation of waste.³³ Therefore, to verify the reusability of 0.5 g-lignin/TiO₂, adsorption tests were carried out in six cycles using the same solid. It was found that the BPA removal capacity remained high (> 70%) until the third cycle, which indicates good stability (Figure 11).

The reduction in adsorption capacity with the increase in number of cycles can be related to the decrease in number of adsorption sites during the adsorption/desorption process due to material losses in the adsorbent regeneration step.⁵⁴ However, despite this reduction, it is notable that the adsorbent can be used in six cycles with significant BPA adsorption capacity.

Characterization of the material after successive adsorption and desorption cycles is expressed in Figure 12. When comparing the FTIR spectrum of the material after recycling (Figure 12a) with the BPA spectrum, the absence

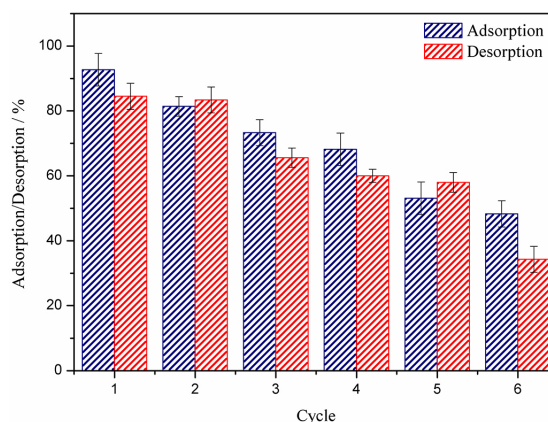


Figure 11. Reuse cycles carried out on the 0.5 g-lignin/TiO₂ composite.

of the band at 1447 cm⁻¹ in the spectrum of the material after recycling indicates that the solvent (methanol) was able to remove BPA from the material.⁵⁰ However, it is also noted that the bands at 3381 and 1616 cm⁻¹ attributed to –OH and –COOH groups, respectively, present on the surface of the composite had disappeared, indicating that methanol may also have solubilized part of these surface groups. The band at 594 cm⁻¹ attributed to Ti–O and Ti–O–Ti bonds is observed in the composite after recycling, and

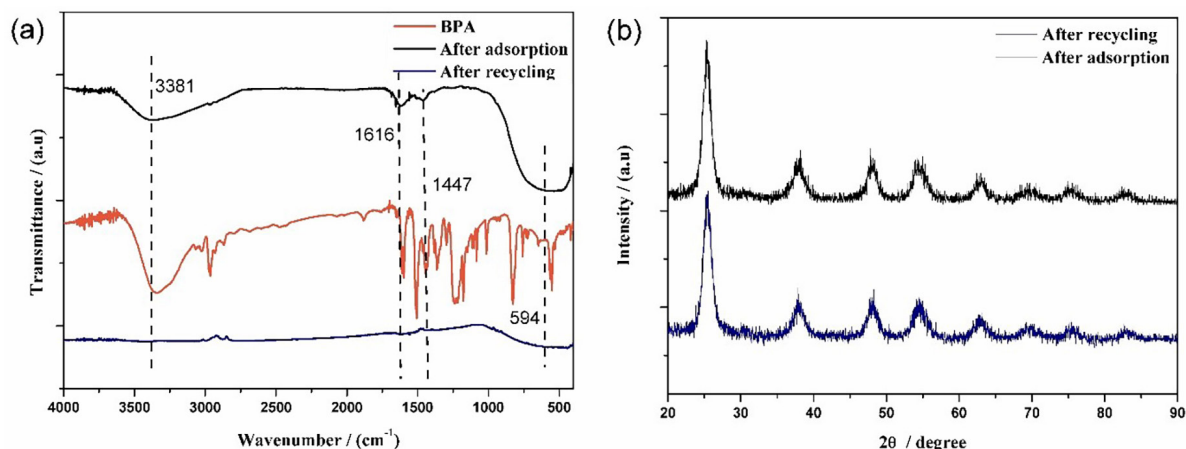


Figure 12. Characterizations of the composite material after successive adsorption and desorption cycles.

the XRD spectra (Figure 12b) reinforce that the anatase phase of TiO₂ was preserved even after successive cycles of adsorption and desorption.⁴⁹

Conclusions

From the characterization results of lignocellulose, it was possible to determine a good percentage of lignin in the sisal residue, which proves that this residue is a source of carbon derived from low-cost and renewable lignin. In addition, its use as a source of lignin will add value and reduce the impact caused by its disposal. Optimization of the lignin extraction process through the sequential chemical treatments achieved an optimal lignin extraction condition with 73% purity. The application of lignin, together with TiO₂, achieved an improvement in surface area properties, with values of > 100 m² g⁻¹ in the synthesized composites; a homogeneous and uniform distribution of particles on the surface of the composites, as observed in the SEM analyses; nanometer-scale particle size, according to the images generated by TEM; and stable charge distribution at neutral pH values, according to zeta potential analyses. Such parameters made it possible to obtain a lignin/TiO₂ adsorbent composite with an adsorption capacity of 13.7 mg L⁻¹ that removed around 97% of the BPA contaminant. The adsorbent recycle tests indicated that the composite has good capacity to be reused in six adsorption cycles, removing over 70% by the third cycle, which indicates good stability.

Thus, the use of lignin extracted from sisal residue with TiO₂ to obtain a composite for the removal of BPA represents advances in the environmental and materials area, using low-cost lignocellulosic biomass, an excellent source of lignin, and good feasibility for extracting lignin, highlighting the importance of these factors for the effective valorization of lignin.

Acknowledgments

This work was supported by PROPESQ/PRPG/UFPB (code project: PVM13514-2020), CNPq, CAPES and MCTIC/CNPq/National Technology-Science Institute for Polysaccharides (code project: 406973/2022-9).

References

- Barreto, S. M. A. G.; Maia, M. S.; Benicá, A. M.; de Assis, H. R. B. S.; Leite-Silva, V. R.; da Rocha-Filho, P. A.; de Negreiros, M. M. F.; de Oliveira Rocha, H. A.; Ostrosky, E. A.; Lopes, P. S.; de Farias Sales, V. S.; Giordani, R. B.; Ferrari, M.; *Ind. Crops Prod.* **2017**, *108*, 470. [Crossref]
- Wang, D.; Li, G.; Zhang, C.; Wang, Z.; Li, X.; *Bioresour. Technol.* **2019**, *289*, 121629. [Crossref]
- Wang, H.; Pu, Y.; Ragauskas, A.; Yang, B.; *Bioresour. Technol.* **2019**, *271*, 449. [Crossref]
- Masilompane, T. M.; Chaukura, N.; Mishra, S. B.; Mishra, A. K.; *Int. J. Biol. Macromol.* **2018**, *120*, 1659. [Crossref]
- Chio, C.; Sain, M.; Qin, W.; *Renewable Sustainable Energy Rev.* **2019**, *107*, 232. [Crossref]
- Boarino, A.; Klok, H.-A.; *Biomacromolecules* **2023**, *24*, 1065. [Crossref]
- Wang, T.; Jiang, M.; Yu, X.; Niu, N.; Chen, L.; *Sep. Purif. Technol.* **2022**, *302*, 122116. [Crossref]
- Zhang, H.; Wang, X.; Ding, H.; *Chem. Phys. Lett.* **2023**, *829*, 140757. [Crossref]
- Zhang, B.; Yang, D.; Lin, W.; Wang, H.; Qian, Y.; Qiu, X.; *J. Ind. Eng. Chem.* **2021**, *97*, 216. [Crossref]
- Wang, H.; Qiu, X.; Liu, W.; Yang, D.; *Appl. Surf. Sci.* **2017**, *426*, 206. [Crossref]
- Shan, X.; Zhao, Y.; Bo, S.; Yang, L.; Xiao, Z.; An, Q.; Zhai, S.; *Sci. Total Environ.* **2021**, *796*, 148984. [Crossref]
- Yang, J.; Dai, J.; Liu, X.; Fu, S.; Zong, E.; Song, P.; *Int. J. Biol. Macromol.* **2022**, *210*, 85. [Crossref]

13. Klapiszewski, Ł.; Siwińska-Stefańska, K.; Kołodyńska, D.; *Chem. Eng. J.* **2017**, *314*, 169. [Crossref]
14. Ohore, O. E.; Zhang, S.; *Sci. Afr.* **2019**, *5*, e00135. [Crossref]
15. Santos, J. S.; Pontes, M. S.; de Souza, M. B.; Fernandes, S. Y.; Azevedo, R. A.; de Arruda, G. J.; Santiago, E. F.; *Chemosphere* **2023**, *343*, 140235. [Crossref]
16. Ramos, R. L.; Lebron, Y. A. R.; Moreira, V. R.; de Souza Santos, L. V.; Amaral, M. C. S.; *Environ. Monit. Assess.* **2021**, *193*, 687. [Crossref]
17. Lee, C.-C.; Jiang, L.-Y.; Kuo, Y.-L.; Hsieh, C.-Y.; Chen, C. S.; Tien, C.-J.; *Chemosphere* **2013**, *91*, 904. [Crossref]
18. Zielińska, M.; Bułkowska, K.; Cydzik-Kwiatkowska, A.; Bernat, K.; Wojnowska-Baryła, I.; *Int. J. Environ. Sci. Technol.* **2016**, *13*, 2239. [Crossref]
19. Yüksel, S.; Kabay, N.; Yüksel, M.; *J. Hazard. Mater.* **2013**, *263*, 307. [Crossref]
20. Sharma, J.; Mishra, I. M.; Kumar, V.; *J. Environ. Manage.* **2015**, *156*, 266. [Crossref]
21. Umar, M.; Roddick, F.; Fan, L.; Aziz, H. A.; *Chemosphere* **2013**, *90*, 2197. [Crossref]
22. Yang, S.; Hai, F. I.; Nghiem, L. D.; Nguyen, L. N.; Roddick, F.; Price, W. E.; *Int. Biodeterior. Biodegrad.* **2013**, *85*, 483. [Crossref]
23. Bhatnagar, A.; Anastopoulos, I.; *Chemosphere* **2017**, *168*, 885. [Crossref]
24. Testing Procedures of Technical Association of the Pulp and Paper Industrial (TAPPI); *TAPPI Standards, Technical Information Papers (TIPS) and Useful Methods*; TAPPI: Atlanta. [Link] accessed in April 2024
25. Xavier, F. D.; Bezerra, G. S.; Santos, S. F. M.; Oliveira, L. S. C.; Silva, F. L. H.; Silva, A. J. O.; Conceição, M. M.; *Biomolecules* **2018**, *8*, 2. [Crossref]
26. Djellabi, R.; Yang, B.; Wang, Y.; Cui, X.; Zhao, X.; *Chem. Eng. J.* **2019**, *366*, 172. [Crossref]
27. Martins, A. C.; Cazetta, A. L.; Pezoti, O.; Souza, J. R. B.; Zhang, T.; Pilau, E. J.; Asefa, T.; Almeida, V. C.; *Ceram. Int.* **2017**, *43*, 4411. [Crossref]
28. Golveia, J. C. S.; Santiago, M. F.; Silva, L. B.; Campos, L. C.; Schimidt, F.; *J. Braz. Chem. Soc.* **2021**, *32*, 1396. [Crossref]
29. de Moraes, N. P.; Campos, T. M. B.; Thim, G. P.; de Siervo, A.; Lanza, M. R. V.; Rodrigues, L. A.; *Chem. Phys. Impact* **2023**, *6*, 100182. [Crossref]
30. Freundlich, H. M. F.; *J. Phys. Chem.* **1906**, *57*, 385. [Crossref]
31. Langmuir, I.; *J. Am. Chem. Soc.* **1918**, *40*, 1361. [Crossref]
32. Vafakhah, S.; Bahrololoom, M.; Saeedikhani, M.; *J. Water Resour. Prot.* **2006**, *8*, 1238. [Crossref]
33. Mamman, S.; Suah, F. B. M.; Raaov, M.; Mehamod, F. S.; Asman, S.; Zain, N. N. M.; *R. Soc. Open Sci.* **2021**, *8*. [Crossref]
34. De Bhowmick, G.; Sarmah, A. K.; Sen, R.; *Bioresour. Technol.* **2018**, *247*, 1144. [Crossref]
35. Kumari, D.; Singh, R.; *Renewable Sustainable Energy Rev.* **2018**, *90*, 877. [Crossref]
36. Ferreira, V. R. A.; Amorim, C. L.; Cravo, S. M.; Tiritan, M. E.; Castro, P. M. L.; Afonso, C. M. M.; *Int. Biodeterior. Biodegrad.* **2016**, *110*, 53. [Crossref]
37. Qian, M.; Lei, H.; Villota, E.; Mateo, W.; Zhao, Y.; Huo, E.; Zhang, Q.; Lin, X.; Huang, Z.; *Bioresour. Technol. Rep.* **2019**, *8*, 100339. [Crossref]
38. Domínguez-Robles, J.; Sánchez, R.; Díaz-Carrasco, P.; Espinosa, E.; García-Domínguez, M. T.; Rodríguez, A.; *Int. J. Biol. Macromol.* **2017**, *104*, 909. [Crossref]
39. Askari, M. B.; Tavakoli Banizi, Z.; Seifi, M.; Bagheri Dehaghi, S.; Veisi, P.; *Optik* **2017**, *149*, 447. [Crossref]
40. Lai, Y.; Li, Z.; Zhang, Y.; Xu, Z.; Wang, F.; Xie, H.; *Sep. Purif. Technol.* **2023**, *325*, 124748. [Crossref]
41. Srisasiwimon, N.; Chuangchote, S.; Laosiripojana, N.; Sagawa, T.; *ACS Sustainable Chem. Eng.* **2018**, *6*, 13968. [Crossref]
42. Taghizadeh-Lendeh, P.; Mohsen Sarrafi, A. H.; Alihosseini, A.; Bahri-Laleh, N.; *Polyhedron* **2023**, *116715*. [Crossref]
43. Lisowski, P.; Colmenares, J. C.; Mašek, O.; Łomot, D.; Chernyayeva, O.; Lisovytskiy, D.; *J. Anal. Appl. Pyrolysis* **2018**, *131*, 35. [Crossref]
44. Liu, G.; Xu, S.; Li, W.; Wang, Z.; Cao, M.; Cui, J.; Jiang, X.; Li, Z.; *J. Solid State Chem.* **2023**, *326*, 124223. [Crossref]
45. Gloria, D. C. S.; Brito, C. H. V.; Mendonça, T. A. P.; Brazil, T. R.; Domingues, R. A.; Vieira, N. C. S.; Santos, E. B.; Gonçalves, M.; *Mater. Chem. Phys.* **2023**, *305*, 127947. [Crossref]
46. Young, T.; Geng, M.; Lin, L.; Thagard, S. M.; *J. Adv. Oxid. Technol.* **2013**, *16*, 89. [Crossref]
47. Valentini, G.; Caon, N. B.; Faita, F. L.; Parize, A. L.; *J. Braz. Chem. Soc.* **2023**, *34*, 167. [Crossref]
48. Sudhakar, P.; Mall, I. D.; Srivastava, V. C.; *Desalin. Water Treat.* **2016**, *57*, 12375. [Crossref]
49. Supong, A.; Bhomick, P. C.; Baruah, M.; Pongener, C.; Sinha, U. B.; Sinha, D.; *Sustainable Chem. Pharm.* **2019**, *13*, 100159. [Crossref]
50. Rani, S.; Sabharwal, H.; Kumar, P.; Chauhan, A. K.; Khoo, K. S.; Kataria, N.; *Groundwater Sustainable Dev.* **2024**, *25*, 101121. [Crossref]
51. Hao, W.; Waisi, B. I.; Vadas, T. M.; McCutcheon, J. R.; *Chin. J. Chem. Eng.* **2023**, *61*, 248. [Crossref]
52. Shi, W.; Wang, H.; Yan, J.; Shan, L.; Quan, G.; Pan, X.; Cui, L.; *Sep. Purif. Technol.* **2022**, *289*, 120796. [Crossref]
53. Yousefinia, S.; Sohrabi, M. R.; Motiee, F.; Davallo, M.; *J. Contam. Hydrol.* **2021**, *243*, 103906. [Crossref]
54. Ghemit, R.; Makhloufi, A.; Djebri, N.; Fililissa, A.; Zerroual, L.; Boutahala, M.; *Groundwater Sustainable Dev.* **2019**, *8*, 520. [Crossref]

Submitted: December 3, 2023

Published online: April 26, 2024